NANO LETTERS

LETTER

pubs.acs.org/NanoLett

Local Electronic Properties of Graphene on a BN Substrate via Scanning Tunneling Microscopy

Régis Decker,[*,†,‡,§] Yang Wang,[†,§] Victor W. Brar,[†,‡] William Regan,[†] Hsin-Zon Tsai,[†] Qiong Wu,[†] William Gannett,[†,‡] Alex Zettl,[†,‡] and Michael F. Crommie[†,‡]

[†]Department of Physics, University of California Berkeley, Berkeley, California 94720, United States

[‡]Materials Science Division, Lawrence Berkeley National Laboratory, Berkeley, California 94720, United States

ABSTRACT: The use of boron nitride (BN) as a substrate for graphene nanodevices has attracted much interest since the recent report that BN greatly improves the mobility of charge carriers in graphene compared to standard SiO_2 substrates. We have explored the local microscopic properties of graphene on a BN substrate using scanning tunneling microscopy. We find that BN substrates result in extraordinarily flat graphene layers that display microscopic Moiré patterns arising from the relative orientation of the graphene and BN lattices. Gate-dependent dI/dV spectra of graphene on BN exhibit spectroscopic features that are sharper than those obtained for graphene on SiO_2. We observe a significant reduction in local microscopic charge inhomogeneity for graphene on BN compared to graphene on SiO_2.

KEYWORDS: Graphene, boron nitride, STM, Moiré

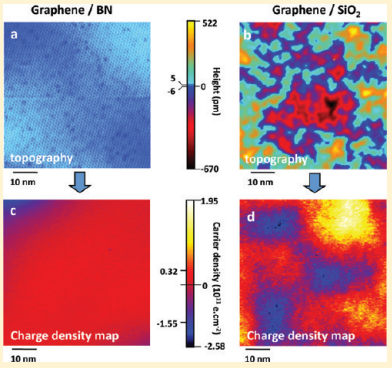

The search for new substrates that improve monolayer graphene properties has been an intense focus of research since graphene was first isolated in 2004.[1] The nature of graphene, a one atom-thick carbon membrane where each atom is exposed to the external environment, makes it highly sensitive to local surroundings, such as substrate curvature, screening, and impurities.[2,3] So far, graphene layers have been prepared on a variety of substrates including SiC,[4,5] metal surfaces,[6,7] mica,[8] and SiO_2.[1,9,10] In the case of SiO_2, the most commonly used substrate for graphene devices, it has been shown that the presence of impurities induces charge density fluctuations that lead to a reduction in electronic mobility.[11] Suspension of graphene membranes has been successfully used to remove the unwanted effects of SiO_2 substrates, but these devices are difficult to fabricate[12] and to measure using scanning probe techniques (which require mechanical stability).[13] It is thus desirable to explore and discover new graphene substrates to attain improved graphene qualities. One such substrate is hexagonal boron nitride (BN), which has a large band gap (5.97 eV[14]), does not have dangling bonds, is relatively inert, presents a low density of charged impurities, and is flat. Transport experiments have shown that graphene/BN has higher mobility than has been observed for graphene/SiO_2.[15,16,11] The local electronic structure of graphene/BN, however, has not yet been explored.

Here, we report a scanning tunneling microscopy (STM) study of the topographic and local electronic structure of graphene monolayers placed on top of hexagonal BN substrates. We observe directly that graphene/BN has significantly enhanced local properties over graphene/SiO_2. One example of this is a dramatic decrease of roughness in the topography of graphene/BN compared to graphene/SiO_2. More importantly, we also measure greatly improved local electronic properties for graphene/BN, such as significantly reduced charge density inhomogeneity in graphene/BN compared to graphene/SiO_2. Whereas graphene/SiO_2 exhibits pervasive charge density fluctuations,[11,16] graphene/BN has a much smoother electronic background with large areas showing extremely low charge density inhomogeneity. Gate-dependent STM spectroscopy of graphene/BN shows clear features of electron−phonon and electron−electron coupling. Some spectroscopic features are sharper and more clearly resolved for graphene/BN than for comparable devices incorporating graphene/SiO_2.

Gated nanodevices incorporating graphene/BN heterostructures were integrated into a low-temperature ultrahigh vacuum (UHV) STM, as shown in Figure 1. BN flakes of average width ∼50 μm and many layers in height were deposited onto SiO_2 by mechanical exfoliation from a commercial BN powder (Momentive Inc.) and annealed at ∼500 °C several hours in air. A clean monolayer of CVD-grown graphene (see ref 17) was subsequently placed on top of the SiO_2/Si wafer decorated by BN flakes. Multiple locations were examined on three distinct graphene/BN devices fabricated in this way. For each case, the graphene layer is grounded via a gold/titanium electrode obtained by e-beam evaporation on the graphene layer using a shadow mask technique.[10] The devices used in our experiments allow a gate voltage to be applied between the graphene layer and the Si electrode, thus enabling tuning of the charge carrier density of graphene.[10] All STM measurements were performed in UHV conditions ($p < 10^{-11}$ Torr) at 4.2 K in an Omicron LT-STM.

Received: February 11, 2011
Published: May 09, 2011

ACS Publications © 2011 American Chemical Society

Completed devices were annealed several hours at ~500 °C in UHV before being transferred in situ to the STM for measurement. Before all STM measurements, the PtIr STM tip was calibrated by measuring the Shockley surface state of an independent Au(111) crystal. STM topographs were acquired in the constant current mode with the bias voltage, V_b, defined as the voltage applied to the sample with respect to the STM tip. STM dI/dV spectra were obtained by lock-in detection of the ac tunnel current induced by a wiggle voltage (5−6 mV rms, 350−500 Hz) added to V_b.

Atomically resolved STM topographs of graphene/BN are shown in Figure 2. Graphene/BN is more locally stable than graphene/SiO_2 as evidenced by the fact that it can be imaged with tunnel currents higher than 2 nA in contrast to graphene/SiO_2 devices which typically become unstable due to tip−surface interactions for $I_T > 1$ nA.[13] This higher stability for graphene/BN indicates more homogeneous bonding between graphene and BN and an absence of small suspended graphene areas that vibrate under the STM tip (as has been reported for graphene/SiO_2[13]). The homogeneity of graphene/BN can also be seen by the extremely flat graphene/BN images shown in Figure 2. The four STM topographs of Figure 2 display different Moiré patterns arising from a lattice mismatch between the graphene layer and the underlying BN surface. The Moiré patterns differ in their lattice size and orientation with respect to the resolved graphene lattice. This difference is attributed to different twisting angles between the graphene and the underlying BN arising from differently rotated graphene grains[18,19] and/or different BN crystallographic orientations within a single flake. Even though the BN lattice is not visible, its twisting angle with respect to graphene can be determined by considering the Fourier transforms of the Moiré pattern as shown in Figure 2e−h. Here the outer spots show the graphene reciprocal lattice and the inner spots indicate the Moiré pattern reciprocal lattice (arrows in Figure 2e). The relative orientation of the BN lattice can be extracted from the relation between reciprocal vectors $\mathbf{k}_{BN} = \mathbf{k}_{graphene} - \mathbf{k}_{Moiré}$ and by assuming a 1.7% difference between the lattice constants of graphene and BN.[20] For a given $\mathbf{k}_{graphene}$, there is a unique relative orientation between the vectors $\mathbf{k}_{graphene}$ and $\mathbf{k}_{Moiré}$, which provides the vector modulus expected for $\mathbf{k}_{BN}$. The relationship between these vectors is shown in Figure 2e. The images in Figure 2 exhibit graphene−BN twisting angles of $\theta = 21 \pm 1°$ (Figure 2a), $\theta = 7 \pm 1°$ (Figure 2b), $\theta = 4 \pm 1°$ (Figure 2c), and $\theta = 0 \pm 1°$ (Figure 2d).

Graphene/BN is characterized by a strong reduction in rms roughness compared to graphene/SiO_2. The rms roughnesses for the Moiré patterns exhibited in Figure 2, for example, are 0.02 Å (Figure 2a), 0.04 Å (Figure 2b), 0.06 Å (Figure 2c), and 0.17 Å (Figure 2d). These roughnesses are much smaller than the roughness typically measured for graphene/SiO_2, which is

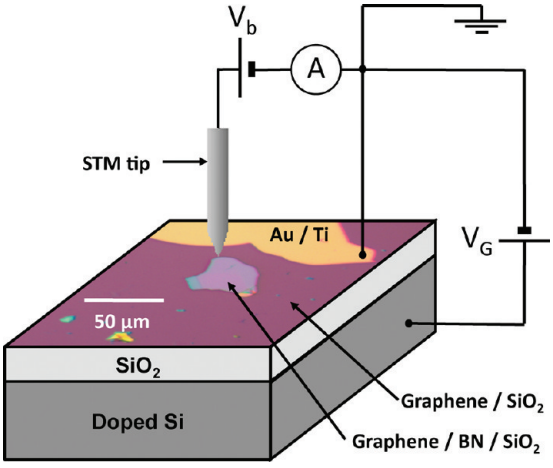

Figure 1. Optical image of graphene/BN device integrated into STM. A CVD-grown graphene layer is mechanically placed over a BN flake set upon a SiO_2 substrate. The graphene is grounded via a gold/titanium electrode. A back-gate voltage V_G is applied to the doped Si electrode.

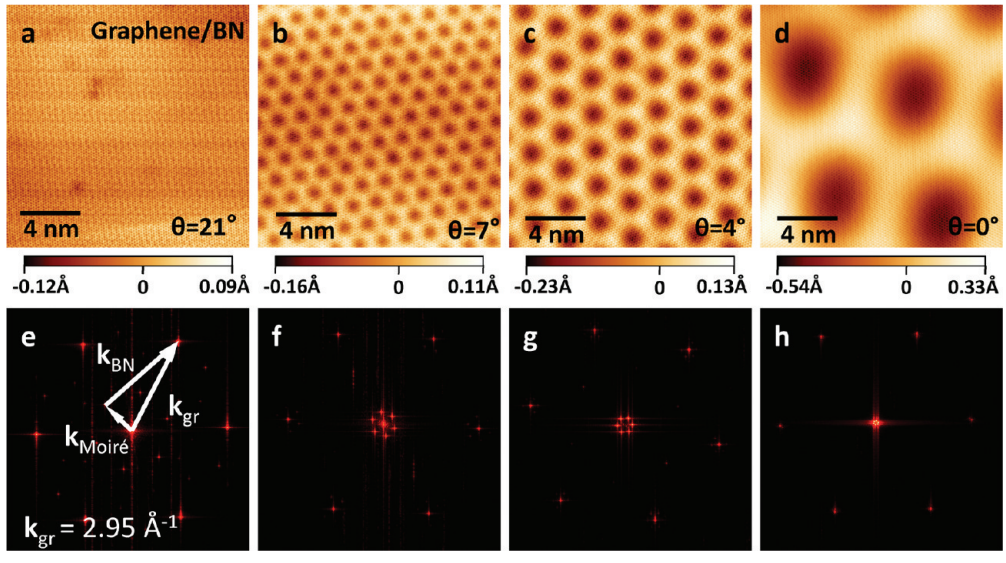

Figure 2. Graphene/BN surface topography. (a−d) The 20 nm × 20 nm constant current STM topographs at four different graphene/BN locations show how the graphene/BN Moiré pattern changes depending on the rotational orientation (θ) between graphene and the BN lattices (see text). (a) $I_T = 0.1$ nA, $V_b = 0.15$ V, $V_G = -25$ V, $\theta = 21 \pm 1°$. (b) $I_T = 0.2$ nA, $V_b = 0.15$ V, $V_G = 0$ V, $\theta = 7 \pm 1°$. (c) $I_T = 0.2$ nA, $V_b = 0.15$ V, $V_G = -6$ V, $\theta = 4 \pm 1°$. (d) $I_T = 0.15$ nA, $V_b = 0.15$ V, $V_G = -3$ V, $\theta = 0 \pm 1°$. (e−h) Fourier transforms of the topographs (a−d). The outer spots show the graphene reciprocal lattice, the inner spots show the graphene/BN Moiré pattern reciprocal lattice.

dx.doi.org/10.1021/nl2005115 |*Nano Lett.* 2011, 11, 2291–2295

approximately 1.5−2.0 Å rms.[10] The latter arises typically from the corrugation of the amorphous underlying SiO_2 substrate[8] and is absent for the crystalline BN substrate. Figure 4a,b shows a side-by-side topographical comparison of typical graphene corrugations on a BN and SiO_2 substrate,[16] respectively, and demonstrates the reduced roughness of graphene/BN over large areas.

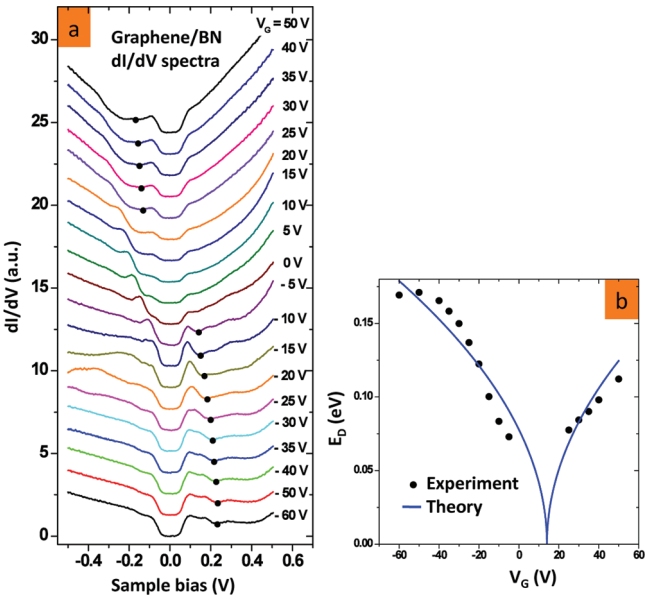

Figure 3. Gate dependence of differential conductance (dI/dV) spectra. (a) Typical STM dI/dV spectra of graphene/BN obtained with tunnel junction impedance = 2.5 GΩ (set point: I_T = 0.2 nA, V_b = −0.5 V). Black dots mark minima in spectra used to extract the Dirac point energy (see text). (b) Black dots: Dirac point energy vs gate voltage extracted from dI/dV spectra (see text). The blue curve is a theoretical fit using the square-root dependence of the Dirac point energy vs gate voltage.

Figure 3 shows STM dI/dV spectra obtained on a graphene/BN device using a set point of I_T = 0.2 nA and V_b = 0.5 V. No significant differences are observed in spectra obtained in this way from different devices or from graphene regions displaying different Moiré patterns. Each spectrum was taken at a different gate voltage, V_G, and thus corresponds to a different charge carrier density in graphene. Similar to previous reports for graphene on SiC,[5] SiO_2,[10] and Pt(111)[2], we observe a gaplike feature of width ∼126 meV at the Fermi energy that does not depend on the charge carrier density. This feature is attributed to the opening of an inelastic tunneling channel via the excitation of out-of-plane phonons at the K/K' points of the graphene reciprocal lattice.[21,22,10]

The Dirac point energy for each spectrum was extracted from the local minimum in dI/dV (black dots in Figure 3a), as calculated from a polynomial fit to the data.[10] The energy of the Dirac point versus the gate voltage is plotted in Figure 3b, where the energy of the inelastic phonon excitation (63 meV) has been subtracted.[10] Points for E_D close to the Fermi energy are not shown due to the absence of a clear Dirac minimum in those spectra because of the influence of the phonon feature in this gate-voltage range. We fitted the Dirac point energy vs the gate voltage with $E_D = \hbar v_F(\pi\alpha|V_G - V_0|)^{1/2}$ where e is the electron charge, V_0 is the gate-voltage offset of the neutral point (V_0 = 14.1 V for the data shown in Figure 3a), v_F is the

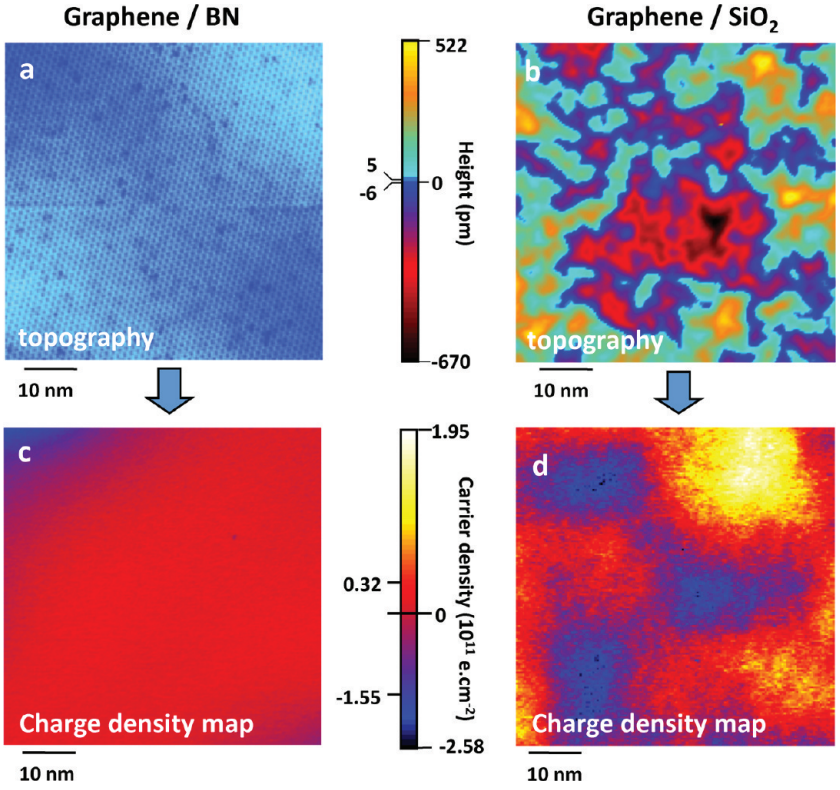

Figure 4. Comparing topography and charge density for graphene/BN vs graphene/SiO_2. (a,b) The 60 nm × 60 nm STM topographs of (a) graphene/BN (I_T = 0.2 nA, V_b = 0.25 V, V_G = −6 V) and (b) graphene/SiO_2 (I_T = 0.02 nA, V_b = −0.225 V, V_G = 15 V). Charge density maps obtained from conductance maps (see text) are shown for (c) graphene/BN (same area as in (a), acquired simultaneously) and (d) graphene/SiO_2 (same area as in (b), acquired simultaneously). The minima and maxima marked in the scales are the minima and maxima of the respective images.

dx.doi.org/10.1021/nl2005115 |*Nano Lett.* 2011, 11, 2291–2295

Fermi velocity (taken as 1.1×10^6 m s^{-1})[10], and α is the capacitance per area. From this fitting we deduce a smaller value for α (3.0×10^{10} cm^{-2} V^{-1} for the data shown in Figure 3a) than was previously seen for graphene/SiO_2 using similar Si wafers (7.1×10^{10} cm^{-2} V^{-1}). This is consistent with the reduction of capacitance expected due to the larger distance between the graphene layer and the Si electrode arising from the additional thickness of the BN flake. We find that V_0 and α vary for different measurements due to changes in the work function of the STM tip[23] as well as differences in the thickness of different BN flakes used for different devices. Our graphene/BN spectra (including the case where the twist angle is $\theta \approx 0°$) do not display any obvious feature indicating the opening of a gap at E_D, as predicted to arise from the breaking of equivalence between graphene atoms when it is perfectly stacked on BN.[20] We observe an enhancement in the spectroscopic peak seen in the range -0.25 V $< V_b < -0.1$ V for low gate voltages (-5 V $< V_G <$ 20 V) compared to graphene/SiO_2 devices.[24] This spectroscopic feature was explained previously as a result of manybody interactions in graphene/SiO_2.[24] The fact that it is more pronounced for graphene/BN suggests a possible difference in electron−electron interactions for graphene/BN compared to graphene/SiO_2 (such as might arise from variations in quasiparticle scattering rates[24]).

Charge density inhomogeneities in graphene/BN are significantly reduced compared to what is observed for graphene/SiO_2. This can be seen in the charge density maps of Figure 4c,d, which were obtained simultaneously with the topographs in Figure 4a,b. Here we have extracted the position-dependent density of charge carriers, $n(x,y)$, from the energy of the Dirac point, $E_D(x,y)$, as follows: $n(x,y) = E_D^2(x,y)/\pi(\hbar v_F)^2$. $E_D(x,y)$ was measured at different positions using a combination of spectral grids and dI/dV maps.[16] Roughness in the graphene/BN charge density for the surface shown in Figure 4c is 2.3×10^{10} e cm^{-2} rms. Corresponding roughness in the graphene/SiO_2 charge density map[16] of Figure 4d is 8.2×10^{10} e cm^{-2} rms, a significantly higher value than found for graphene/BN. This suggests a smaller density of charged impurities for the graphene/BN system.[16] We also note that no intravalley quasiparticle interference patterns[25,26] were observed on pristine graphene/BN, contrary to what is observed for graphene/SiO_2,[16] again consistent with a reduction in electronic scatterers for the graphene/BN system.

In conclusion, our results show direct microscopic evidence that graphene/BN improves graphene stability, roughness, and intrinsic local electronic properties compared to graphene/SiO_2. The variable Moiré patterns observed here might be exploited as periodic potential networks for patterning atomic or molecular adsorbates.[7,27] The smaller charge fluctuations and reduced scattering seen for graphene/BN show that BN substrates provide a promising route for investigating the intrinsic local behavior of graphene.

AUTHOR INFORMATION

Corresponding Author

*E-mail: regis.decker@gmail.com

Author Contributions

§These authors contributed equally to this work.

ACKNOWLEDGMENT

STM instrumentation development and measurements supported by the Director, Office of Science, Office of Basic Energy Sciences, Division of Materials Sciences and Engineering Division, U.S. Department of Energy under Contract No. DE-AC03-76SF0098; BN substrate fabrication and graphene growth supported by Office of Naval Research MURI Program Award No. N00014-09-1-1066; STM data analysis supported by the National Science Foundation under Grant DMR-0906539; R.D. acknowledges a fellowship from the Swiss National Science Foundation (Grant PBELP2-122886).

REFERENCES

(1) Novoselov, K. S.; Geim, A. K.; Morozov, S. V.; Jiang, D.; Zhang, Y.; Dubonos, S. V.; Grigorieva, I. V.; Firsov, A. A. *Science* **2004**, *306*, 666–669.

(2) Levy, N.; Burke, S. A.; Meaker, K. L.; Panlasigui, M.; Zettl, A.; Guinea, F.; Castro Neto, A. H.; Crommie, M. F. *Science* **2010**, *329*, 544–547.

(3) Castro Neto, A. H.; Guinea, F.; Peres, N. M. R.; Novoselov, K. S.; Geim, A. K. *Rev. Mod. Phys.* **2009**, *81*, 109–162.

(4) Berger, C.; Song, Z.; Li, X.; Wu, X.; Brown, N.; Naud, C.; Mayou, D.; Li, T.; Hass, J.; Marchenkov, A. N.; Conrad, E. H.; First, P. N.; de Heer, W. A. *Science* **2006**, *312*, 1191–1196.

(5) Brar, V. W.; Zhang, Y.; Yayon, Y.; Ohta, T.; McChesney, J. L.; Bostwick, A.; Rotenberg, E.; Horn, K.; Crommie, M. F. *Appl. Phys. Lett.* **2007**, *91*, No.122102.

(6) Marchini, S.; Günther, S.; Wintterlin, J. *Phys. Rev. B* **2007**, *76*, No. 075429.

(7) N'Diaye, A. T.; Bleikamp, S.; Feibelman, P. J.; Michely, T. *Phys. Rev. Lett.* **2006**, *97*, No. 215501.

(8) Lui, C. H.; Liu, L.; Mak, K. F.; Flynn, G. W.; Heinz, T. F. *Nature* **2009**, *462*, 339–341.

(9) Zhang, Y.; Tan, Y.-W.; Stormer, H. L.; Kim, P. *Nature* **2005**, *438*, 201–204.

(10) Zhang, Y.; Brar, V. W.; Wang, F.; Girit, C.; Yayon, Y.; Panlasigui, M.; Zettl, A.; Crommie, M. F. *Nat. Phys.* **2008**, *4*, 627–630.

(11) Martin, J.; Akerman, N.; Ulbricht, G.; Lohmann, T.; Smet, J. H.; von Klitzing, K.; Yacoby, A. *Nat. Phys.* **2007**, *4*, 144–148.

(12) Du, X.; Skachko, I.; Barker, A.; Andrei, E. Y. *Nat. Nanotechnol.* **2008**, *3*, 491–495.

(13) Marshoff, T.; Pratzer, M.; Geringer, V.; Echtermeyer, T. J.; Lemme, M. C.; Liebmann, M.; Morgenstern, M. *Nano Lett.* **2010**, *10*, 461–465.

(14) Watanabe, K.; Taniguchi, T.; Kanda, H. *Nat. Mater.* **2004**, *3*, 404–409.

(15) Dean, C. R.; Young, A. F.; Meric, I.; Lee, C.; Wang, L.; Sorgenfrei, S.; Watanabe, K.; Tanigushi, T.; Kim, P.; Shepard, K. L.; Hone, J. *Nat. Nanotechnol.* **2010**, *5*, 722–736.

(16) Zhang, Y.; Brar, V. W.; Girit, C.; Zettl, A.; Crommie, M. F. *Nat. Phys.* **2009**, *6*, 722–726.

(17) Li, X.; Cai, W.; An, J.; Kim, S.; Nah, J.; Yang, D.; Piner, R.; Velamakanni, A.; Jung, I.; Tutuc, E.; Banerjee, S. K.; Colombo, L.; Ruof, R. S. *Science* **2009**, *324*, 1312–1314.

(18) Huang, P. Y.; Ruiz-Vargas, C. S.; van der Zande, A. M.; Whitney, W. S.; Levendorf, M. P.; Kevek, J. W.; Garg, S.; Alden, J. S.; Hustedt, C. J.; Zhu, Y.; Park, J.; McEuen, P. L.; Muller, D. A. *Nature* **2011**, *469*, 389–393.

(19) Kim, K.; Lee, Z.; Regan, W.; Kisielowski, C.; Crommie, M. F.; Zettl, A. *ACS Nano* **2011**, *5* (3), 2142–2146.

(20) Giovannetti, G.; Khomyakov, P. A.; Brocks, G.; Kelly, P. J.; van der Brink, J. *Phys. Rev. B* **2007**, *76*, No. 073103.

(21) Mohr, M.; Maultzch, J.; Dobardzic, E.; Reich, S.; Milosevic, I.; Damnjanovic, M.; Bosak, A.; Krisch, M.; Thomsen, C. *Phys. Rev. B* **2007**, *76*, No. 035439.

(22) Wehling, T. O.; Grigorenko, I.; Lichtenstein, A. I.; Balatsky, A. V. *Phys. Rev. Lett.* **2008**, *101*, No. 216803.
(23) Brar, V. W.; Decker, R.; Solowan, H.-M.; Wang, Y.; Maserati, L.; Chan, K. T.; Lee, H.; Girit, C.; Zettl, A.; Louie, S. G.; Cohen, M. L.; Crommie, M. F. *Nat. Phys.* **2011**, *7*, 43–47.
(24) Brar, V. W.; Wickenburg, S.; Panlasigui, M.; Park, C.-H.; Wehling, T. O.; Zhang, Y.; Decker, R.; Girit, C.; Balatsky, A. V.; Louie, S. G.; Zettl, A.; Crommie, M. F. *Phys. Rev. Lett.* **2010**, *104*, No. 036805.
(25) Crommie, M. F.; Lutz, C. P.; Eigler, D. *Nature* **1993**, *363*, 524–527.
(26) Rutter, G. M.; Crain, J. N.; Guisinger, N. P.; Li, T.; First, P. N.; Stroscio, J. A. *Science* **2007**, *317*, 219–222.
(27) Brune, H.; Giovannini, M.; Bromann, K.; Kern, K. *Nature* **1998**, *394*, 451–453.
(28) Xue, J.; Sanchez-Yamagishi, J.; Bulmash, D.; Jacquod, P.; Deshpande, A.; Watanabe, K.; Taniguchi, T.; Jarillo-Herrero, P.; LeRoy, B. J. *Nat. Mater.* **2011**, *10*, 282–285.

NOTE ADDED IN PROOF

After submission of the manuscript, we became aware of a related work (ref 28).

NOTE ADDED AFTER ASAP PUBLICATION

This paper published May 9, 2011 with an incorrect version of Figure 1, and an error in data presented in the second to last paragraph of the article. The correct version published May 12, 2011.